On-line Determination of Aggregate Size and Morphology in Suspensions

Frédéric Gruy, Michel Cournil

ON-LINE DETERMINATION OF AGGREGATE SIZE AND MORPHOLOGY IN SUSPENSIONS

Frédéric Gruy[1] and Michel Cournil[2*]

(1) Dr Frédéric Gruy, Ecole des Mines de Saint-Etienne, Dept SPIN, URA CNRS 2021, 158, Cours Fauriel, 42023 F-Saint-Etienne Cedex 2 (France) ; gruy@emse.fr

(2) Prof . Michel Cournil, Ecole des Mines de Saint-Etienne, Dept SPIN, URA CNRS 2021, 158, Cours Fauriel, 42023 F-Saint-Etienne Cedex 2 (France) ; cournil@emse.fr

(*) corresponding author

Abstract

Information about the aggregation state of fine solid particles is an important element for process control and product quality monitoring in many situations of industrial slurries. This work deals with the application of different in line methods to the characterization of silica aggregate size and morphology. All these methods exploit turbidity signals, obtained, however differently: respectively, from turbidity fluctuations analysis in homogeneous suspension and from turbidity global decrease during particle settling. This work gives us also the opportunity to progress in morphological and optical models of small aggregates. Thanks to these models, the aggregate morphological characteristics and the number of their constituting particles are derived from experimental results. Agreement between the different methods is examined and discussed.

1 Introduction

Large aggregates frequently present a fractal structure [1], for instance when they are produced by Brownian aggregation of nanoparticles. Fractal-like objects are also observed during agglomeration in stirred crystallisers. An aggregate containing i primary particles of radius a_1 is typically characterised by its fractal dimension D_f, its outer radius a_i, its hydrodynamic radius a_{Hi}; as the structure of these aggregates is non-uniform, their local volume density $\phi_{i,a}(r)$ depends on the distance r from their centre of mass. The average volume density is denoted $\bar{\phi}_{i,a}$. These different characteristics are linked by the following equations:

$$a_i = a_1\left(\frac{i}{S}\right)^{\frac{1}{D_f}} \tag{1}$$

$$\phi_{i,a}(r) = \frac{S}{3} D_f \left(\frac{r}{a_1}\right)^{D_f - 3} \tag{2}$$

$$\bar{\phi}_{i,a} = S\left(\frac{a_i}{a_1}\right)^{D_f - 3} \tag{3}$$

where S is a structure factor.

From computer simulations, Gmachowski [2-3] found the following correlation between S and D_f for D_f >1.5:

$$S \approx 0.42\, D_f - 0.22 \tag{4}$$

In stirred tank, aggregates are most of the time small and fragile objects, particularly when absence of solubility or supersaturation does not lead to aggregate cementation by crystalline bridges and thus to their strengthening. In most experiments, the aggregate size does not

exceed a maximum value which may result from the dynamic balance between aggregation and fragmentation [4-5].

Small aggregates cannot be considered as fractal-like objects. One of us [6], nevertheless, proposed to keep relation (1), however, by replacing outer radius a_i by an equivalent radius $a_{i,e}$ which is defined from the projected area S_p on a plane of the moving aggregate by relation:

$$\pi a_{i,e}^2 = \left\langle S_p \right\rangle_O \tag{5}$$

in which $\left\langle S_p \right\rangle_O$ is the average of the projected area on all aggregate orientations. In aggregation and sedimentation models, indeed, S_p is an important relevant parameter.

The corresponding average volume density is:

$$\bar{\phi}_{i,e} = i\left(\frac{a_1}{a_{i,e}}\right)^3 \tag{6}$$

Assimilating then $\bar{\phi}_{i,e}$ to $\bar{\phi}_{i,a}$ thanks to Eq. (3), *weak fractal dimension* D_{wf} can be defined [6]. This is a more realistic definition than the fractal dimension extrapolation to small aggregates. In [6] we proved for instance that silica aggregates in a stirred tank were small and slightly porous with weak fractal dimension D_{wf} in the range [2.35-2.45].

Hydrodynamic radius of aggregates is also an important parameter which characterises the aggregate motion in fluid flow. Modelling of fluid flow around and across a large aggregate takes into account its porosity and permeability. Calculation of drag coefficient has been achieved for aggregates with homogeneous porosity and for fractal-like aggregates [7]. Such determinations are difficult to transpose to small aggregates for which internal porosity or permeability cannot be properly defined. So, we performed measurements of drag coefficient of macroscopic aggregates consisting in *i* one-millimetre glass beads with *i* ranging between 2

and 100 [8]. The largest aggregates (30< i <100) could be characterized by D_{wf} values close to 2.5 and their drag coefficient calculated through macroscopic models. For the smallest chosen aggregates (i < 11), however, porosity and permeability are properties without real meaning. Drag coefficient was then calculated from settling measurements in glycerol in order to keep the flow Stokesian nature which exists around micrometric particles in a crystalliser. We showed that the hydrodynamic radius of these aggregates was practically equal to the radius calculated from the average projected area over all orientations, i.e.:

$$a_{Hi} \approx a_{i,e} \tag{7}$$

As expected, effect of porosity on drag coefficient is negligible. Hence, the obtained results express the influence of external shape and roughness of the body on the drag coefficient.

Relation (7) will be used for the general study of aggregate sedimentation in addition to others.

Settling velocity v of a small aggregate at low Reynolds number (Re < 1) is given by [8]:

$$v = v_1 \frac{i}{\beta} \tag{8}$$

$$\text{with } \beta = \frac{a_{i,e}}{a_1} = \left(\frac{i}{S}\right)^{\frac{1}{D_{wf}}} \tag{9}$$

v_1, the settling velocity of a spherical primary particle, is given by Stokes law:

$$v_1 = \frac{2}{9} \Delta\rho \frac{a_1^2 g}{\mu} \tag{10}$$

g, μ and $\Delta\rho$ are respectively the gravity, the liquid dynamic viscosity and the density difference between material and fluid.

For fundamental reasons as well as for process monitoring purpose, real time knowledge of the aggregate size and morphology may be very useful. For these determinations, both on-line and in-line methods can be envisaged. Off-line methods, however, do not ensure isokinetic

withdrawal, particularly, for small particles, and may damage fragile aggregates. In situ techniques would be certainly ideal; however, they are rare and need to be validated. Turbidimetry has been proved to be a particularly efficient method for in situ particle size measurements [9], particularly in aggregating systems [4]. Turbidimetry is based on light scattering by suspensions and rests on the Mie theory [10]. Since the works of Wessely *et al.* [11], analysis of turbidity fluctuations has been shown as particularly interesting for the determination of particle number and size; this principle has given rise to commercial instruments.

Present work is devoted to the characterization of aggregates of silica formed in a stirred vessel. Final aggregates are characterized by their morphology, i.e. weak fractal dimension and number L of primary particles per aggregate. Aggregation itself has been studied by in situ turbidimetry [6, 12]. Final aggregates are characterized both using turbidity fluctuations and settling velocity measurements. Interpretation of these data requires preliminary theoretical tasks: morphological modelling of the aggregates and calculation of their light scattering cross section and their drag coefficient (or hydrodynamic radius). Comparison between L number respectively given by each method is presented and commented on.

2 Experimental part

2.1 Materials, techniques and procedure

Aggregation experiments are performed on samples of monodisperse silica spheres (0.5µm and 1.5 µm in diameter, *Geltech Inc* products). Aggregation is studied in water at pH values 2 to 4 [6, 12]. The solids volume fraction is equal to $7.54\ 10^{-5}$.

The reactor used for this study of aggregation is a stirred tank the diameter of 120 mm in diameter (Figure 1). This reactor is equipped with four baffles. Liquid depth in the vessel is equal to diameter. Bottom part of the tank is rounded. Agitation is ensured by a four bladed

45° Teflon impeller of diameter 60 mm. Temperature is kept constant at 25.00°C ± 0.01°C by a double-wall jacket. The reactor is fitted with an optical system to measure in situ the suspension turbidity in the wavelength range 350 nm-800 nm; its aperture angle is equal to 1.5°.

Aggregation of silica sample is performed in the reactor at given stirring rate for two hours.

- *spectral turbidimetry*

Turbidity τ expresses the extinction phenomenon of an incident light beam due to light scattering by solid particles; it is defined by relation:

$$\tau(\lambda_0) = \frac{1}{L_{opt}} \ln\left(\frac{I_0(\lambda_0)}{I(\lambda_0)}\right) \tag{11}$$

in which λ_0, is the wavelength, $I_0(\lambda_0)$ the intensity of the incident beam and $I(\lambda_0)$ the intensity of the transmitted beam after an optical path of length L_{opt}.

For an aggregate suspension the turbidity contains the contribution of each class of aggregates:

$$\tau(\lambda_0) = \sum_{i=1}^{N} C_{ext,i} N_i \tag{12}$$

where N_i is the number concentration of aggregates consisting in i primary particles and $C_{ext,i}$ is the aggregate extinction cross section.

Calculation of the extinction cross section C_{ext} is relatively easy for spherical [10], compact, or large particles, however much more delicate for small, non compact aggregates [6]. From equation (12), it appears that variations in the aggregate number concentration N_i result in turbidity variation. For instance, in the case of 1.5 μm silica particles in water, turbidity decreases with aggregation, whereas it increases in the case of 0.5 μm particles. When particles leave the measurement cell, due to settling for instance, turbidity decreases obviously. These characteristics will be exploited later on.

- *turbidity fluctuations analysis*

Turbidity fluctuations measurements are performed using Aello 4000 equipment (GWT-TU Dresden, Germany).

Aello 4000 measurement cell is external to the reactor and located on a re-circulation loop; thus measurements are in line and not in situ as previously. This apparatus delivers the turbidity signal of the suspension located in its measurement cell, however with a special interest in the signal fluctuations around its mean value. These fluctuations are due to the fluctuating particle number in the light beam. From statistical analysis of these fluctuations and optical models, mean extinction section $\overline{C}_{ext}$ and particle number $\overline{N}$ in the cell are deduced. This method is only suitable for large particles. The size range of validity is [1µm-500µm]. The aperture angle is equal to 2.5°. Figure 2 shows an example of the signal which is delivered by this apparatus.

Compared to the in situ determinations, this measurement procedure is liable to damage the aggregates, however this effect is certainly reduced because shear stress in the loop is considerably lower than in the reactor and pumping conditions are relatively smooth. This is confirmed by the identical turbidity levels observed in the two experimental systems.

Suspension is pumped to the Aello 4000 cell and characterized during all the aggregation process and at its end.

- *sedimentation velocity measurements*

For characterizing the suspension obtained after two hours of aggregation process, agitation is stopped, however, turbidity keeps on being recorded. The turbidity probe is vertically located at the two-thirds of the vessel radius halfway between two baffles, and mounted at 4.8 cm from the upper surface of the liquid. As soon as agitation is stopped, aggregates start settling and gradual decrease in turbidity is clearly observed (Figure 3).

In ideal case of monodisperse aggregates, the turbidity signal keeps constant for a while and sharply decreases only when the aggregates initially located near the liquid surface have crossed the measurement window. In case of polydisperse aggregates, settling results in a classification of the aggregates according to their size and turbidity drop is not as sharp. Thus, according to the aggregate population nature, different turbidity plots against time are observed (Figure 4). In Figure 4, we have represented the initial turbidity decrease due to aggregation in the stirred vessel in the time interval [0, t_0 = 2 hours] then the turbidity decrease due to sedimentation. Cases a and b are relative to monodisperse aggregates; case c, relative to polydisperse aggregates, is the most commonly observed.

From experimental curves similar to plots of Figure 4a and 4b, we can easily calculate the sedimentation velocity v by dividing the sensor mean depth from the top of the liquid (here H_S = 4.8 cm) by the settling duration. This has been done for silica particles in conditions of non aggregation (pH = 8) and good agreement has been found (using Equation 10). For experimental plots similar to Figure 4c, we have to define a characteristic settling time to be able to determine the aggregate size. This will be discussed further.

2.2 Experimental results

- *sedimentation velocity measurements*

Using procedure described in section 2.1, we obtain turbidity variation when agitation is stopped in the reactor after two hours aggregation. Plots of Figures 5a-b have the same shape as plot of Figure 4c. For micrometric particles, however, the sedimentation time distribution is not only due to suspension polydispersity at initial time, but also to Brownian aggregation or settling aggregation, indeed, which may occur during sedimentation and disturb it.

In order to obtain a corrected sedimentation time, we propose first a simplified model of Brownian aggregation influence on sedimentation before analysing sedimentation experiments.

We consider a suspension composed of monosized aggregates (primary particles number per aggregate $\bar{i}_0$) produced by turbulent aggregation; its volume fraction in solid is denoted ϕ. It is assumed that the suspension remains monodisperse during sedimentation and Brownian aggregation. At a given time, the suspension consists of aggregates with *j* primary aggregates, i.e with $j\bar{i}_0$ primary particles, and is characterized by its aggregate concentration by number *N*. We denote by $D_{f,B}$ and $D_{f,T}$ respectively the fractal dimension of Brownian and turbulent aggregates. The suspension is also considered as spatially homogeneous.

Brownian aggregation kinetics (monodisperse suspension) is described by [1]:

$$\frac{dN}{dt} = -\frac{1}{2}kN^2 \qquad \text{with } k = \frac{4k_B T}{3\mu}$$

T is the temperature, k_B the Boltzmann constant.

Thus, characteristic time T_{Ba} for Brownian aggregation is:

$$T_{Ba} = \frac{4}{3}\pi a_1^3 \bar{i}_0 \frac{2}{k\phi} \tag{13}$$

Sedimentation height H_S (distance between the reactor top and the sensor) and sedimentation time T_S are linked by:

$$H_S = \int_0^{T_S} v(j, D_{f,B})dt$$

with $v\left(j, D_{f,B}\right) = v\left(\bar{i}_0, D_{f,T}\right) j\left(\frac{j}{S}\right)^{-1/D_{f,B}}$ and $j = \frac{\phi}{N\frac{4}{3}\pi a_1^3 \bar{i}_0}$

thus, the relation between the sedimentation time T_S (with Brownian aggregation) and the sedimentation time $T_{S,0}$ (without Brownian aggregation):

$$\frac{T_S}{T_{Ba}} = \left(1 + \alpha\frac{T_{S,0}}{T_{Ba}}\right)^{1/\alpha} - 1 \qquad \text{with } \alpha = \frac{2D_{f,B} - 1}{D_{f,B}} \tag{14}$$

and $T_{S,0} = \frac{H_S}{v_1 \bar{i}_0} \left(\frac{\bar{i}_0}{S} \right)^{1/D_{f,T}}$ (15)

Consequently, sedimentation time T_S is found as a function of sedimentation time $T_{S,0}$ in absence of aggregation, of characteristic time T_{Ba} of Brownian aggregation and of fractal dimension $D_{f,B}$ of the Brownian aggregates. The fractal dimension of Brownian aggregates with occurrence of aggregate restructuring (which is likely here) is about 2.1 [13].

Another cause of aggregation of a polydisperse suspension in a still medium is the collision of aggregates with different settling velocities. The differential settling aggregation kinetics is described by the following relations [1]:

$$\frac{dN_{i+j}}{dt} = -kN_i N_j \quad (16)$$

with $k = \frac{2\pi}{9} \Delta\rho \frac{g}{\mu} \left| a_i^2 - a_j^2 \right| \left(a_i + a_j \right)^2$ (17)

Characteristic time T_{sa} for settling aggregation is still given by Eqn (13).

If we take the example of a polydisperse suspension of size range: $\frac{1}{2}\bar{i}_0 < i < \frac{3}{2}\bar{i}_0$, then

$$\bar{k} = \frac{2\pi}{9} \Delta\rho \frac{g}{\mu} a_i^4 \left(\frac{\bar{i}_0}{S} \right)^{\frac{4}{D_{f,T}}} \left(\left(\frac{3}{2} \right)^{\frac{2}{D_{f,T}}} - \left(\frac{1}{2} \right)^{\frac{2}{D_{f,T}}} \right) \left(\left(\frac{3}{2} \right)^{\frac{2}{D_{f,T}}} + \left(\frac{1}{2} \right)^{\frac{2}{D_{f,T}}} \right)^2 \quad (18)$$

Taking typical value of 2.4 for $D_{f,T}$ [5] and using Eqns (13) and (18), we obtain:

$$\bar{k} = \frac{2\pi}{9} 4.67 \Delta\rho \frac{g}{\mu} a_i^4 \bar{i}_0^{1.67} \quad (19)$$

thus:

$$T_{sa} = \frac{1.29\mu}{\Delta\rho g a_1 \bar{i}_0^{0.67} \varphi} \quad (20)$$

The previous two models either overlook or simplify the polydisperse character of the settling suspension. However, they are useful for a rough estimation of the influence of Brownian and settling aggregation on sedimentation.

For the two silica suspensions, Table 1 contains calculated sedimentation time T_{s0} for typical $\bar{i}_0$ values [6], characteristic times of Brownian aggregation T_{Ba}(Equation 13) and settling aggregation T_{Sa} (Equation 20). We can easily conclude that Brownian aggregation has little effect on sedimentation even for silica 0.5μm. On the contrary, settling aggregation may considerably change the aggregate size initial distribution. Consequently, the distribution tail of the settling times should correspond to the smallest aggregates, i.e. which are present at the end of turbulent aggregation and have not undergone further aggregation in still medium.

As aforesaid in section 2.1, characteristic time of settling should be defined. Then, taking into account the existence of a main "sedimentation wave" on the different plots of Figures 5a-b we chose characteristic sedimentation times corresponding to the end of this wave.

- 0.5 μm silica

Table 2a shows the different settling times and normalized settling velocity v/v_1 obtained for different stirring rates. Using theoretical results of section 1 (Eqns 8-10), we can predict the normalized settling velocity of aggregates of given number of primary particles and fractal dimension. As likely fractal dimension for turbulent aggregation $D_{f,T} = D_{wf}$ is in the range [2.35-2.45] the corresponding number $\bar{i}_0$ of primary particles per aggregate can be deduced.

- 1.5 μm silica

Table 2b shows the different settling times and normalized settling velocity v/v_1 obtained for different stirring rates. The same approach as above leads to the corresponding number $\bar{i}_0$ of primary particles per aggregate (Table 2b).

- *turbidity fluctuations analysis*

As aforesaid, the Aello 4000 equipment allowed us to obtain C_{ext} and number n of particles in the cell at any time, in particular, initial total number of silica primary particles prior to aggregation n_0 is known. Dividing n_0 by n gives us L the mean number of silica particles per

aggregate. Moreover, one can calculate L value by using the relation between light extinction cross section and aggregate geometry. The aperture angle is taken into account for the calculation of light scattering cross-sections [6].

- 0.5 μm silica

at zero time, n_0 and $C_{ext,1}$ are respectively equal to 127500 and $0.0316\mu m^2$ (this latter value comes from Mie theory applied to a spherical body). Light scattering by aggregate composed of 0.5 μm silica particles follows the theory of Effective Refractive Index [6].

- 1.5 μm silica

at zero time, n_0 and $C_{ext,1}$ are respectively equal to 6000 and $1.68\mu m^2$. Light scattering by aggregate composed of 1.5 μm silica particles follows the theory of anomalous diffraction [10].

Corresponding data are reported in Tables 3a-b for different stirring rate values.

Optical microscopy and image analysis

Attempts of aggregate removal after 2 hours aggregation have been made. After their withdrawal with a pipette, the samples have been carefully dried, then observed with a microscope coupled with an image analyser (Zeiss Axioskop microscope, magnification x500; video camera JVC KY-F58; Leica Q-win software). Photographs of the removed samples have been processed in order to determine the number of primary particles per aggregate. Results are reported in Tables 4a-b.

3. Discussion and conclusion

Tables 4a-b compare the estimations of particle number in small silica aggregates using the different methods.

In previous work [6], we showed that aggregation dynamics modelling requires fitting of two physical parameters: weak fractal dimension and the number L of primary particles per

aggregate at steady state. Last row in Tables 4a-b contains the L values coming from this modelling when applied the present silica samples aggregation; details can be found in [12].

Examining the aggregate size estimations reported in Tables 4a-b, we can draw the following conclusions:

i) aggregate sizes obtained from turbidity fluctuation analysis are similar whatever the calculation method (from C_{ext} or from n_0/n); this implies that our light scattering models applied to small aggregates are validated

ii) turbidity fluctuations and settling velocities analysis are quite convergent and indicate that particle number in aggregates composed of micrometric silica particles and formed in stirred tank is relatively low. As the validity range of Aello equipment is between 1 and 250 μm, agreement is better for 1.5 μm particles than for 0.5 μm particles.

iii) direct measurements on withdrawn samples are very different and certainly non representative. They confirm the well known difficulty of isokinetic removal of small objects.

iv) L values coming from aggregation modelling are in qualitative agreement with ones from settling experiments and turbidity fluctuations analysis.

From different experimental works (for instance, [14]), it appears that the normalized maximum particle size $\frac{a_L}{a_1}$ depends on shear rate, according to relation:

$$\frac{a_L}{a_1} \propto \dot{\gamma}^{-c} \qquad \text{with } 0 < c < 1 \qquad (21)$$

Mean gradient velocity $\dot{\gamma}$ in a stirred tank is a function of mean energy dissipation rate ε and kinematic viscosity ν:

$$\dot{\gamma} \propto \left(\frac{\varepsilon}{\upsilon}\right)^{1/2} \tag{22}$$

Many expressions are found in the literature for the mean value of ε, for instance [15]:

$$\varepsilon = \frac{N_p \omega^3 D_S^5}{V}$$

N_p is the power number, D_s the stirrer diameter, ω the rotation rate of the stirrer and V the volume of the suspension.

Thus, $\frac{a_L}{a_1} \propto \omega^{\frac{3c}{2}}$ or $L \propto \omega^{\frac{3c}{2} D_f}$ (23)

Using the results of the present study (Tables 4a-b), we can verify relation (23) in our case and determine exponent c. Good agreement is found, which validates the mathematical form of equation (19) and respective values of c are: 0 (0.5 μm, settling data), 0.23 (0.5 μm, turbidity fluctuation analysis), 0.2 (1.5 μm, the two methods).

REFERENCES

[1] M. Elimelech, J. Gregory, X. Jia, R. Williams, *Particle Deposition & Aggregation*, Butterworth-Heinemann Edt, Oxford, **1995**.

[2] L. Gmachowski, *J. Coll. Interface Sci*., **1996**, *178*, 80

[3] L. Gmachowski, *Colloids and Surfaces A: Physicochemical and Engineering Aspects*, **2000**, *170*, 209.

[4] H. Saint-Raymond, F. Gruy, M. Cournil, *J. Coll. Inter. Sci*., **1998**, *202*, 238.

[5] C. Tontrup, F. Gruy, M. Cournil, *J. Coll. Inter. Sci.*, **2000**, *229*, 511.

[6] F. Gruy, *J. Coll. Inter. Sci*., **2001**, *237*, 28.

[7] M. Vanni, *Chem. Eng. Sci*., **2000**, *55*, 685.

[8] F. Gruy, P. Cugniet, *J. Coll. Inter. Sci.*, in press

[9] G.M. Crawley, M. Cournil, D. Di Benedetto, *Powder Technol*. **1997**, *91*, 197.

[10] H.C. Van de Hulst, *Light Scattering by Small Particles*, Wiley, New York, **1957**.

[11] B. Wessely, J. Altmann, and S. Ripperger, *Chem. Eng.Technol.*, **1996**, *19*, 438.

[12] P. Cugniet, *PhD Thesis*, Ecole des Mines de Saint-Etienne (France), **2003**.

[13] A. Thill, S. Veerapaneni, B. Simon, M. Wiesner, J.Y. Bottero, D. Snidaro, *J. Coll. Inter. Sci.*, **1998**, *204*, 357.

[14] V. Oles, *J. Coll. Inter. Sci.*, **1992**, *154*, 351.

[15] S. Kresta, *Can. J. Chem. Eng.*, **1998**, *76*, 563.

Legends of Figures

Figure 1: Schematic representation of the aggregation reactor

Figure 2: Extinction cross section versus time obtained by turbidity fluctuations analysis for 1.5 μm silica particles (pH = 8)

Figure 3: Aggregate settling as detected by the turbidity sensor

Figure 4: Turbidity variation during aggregate sedimentation; a: large monodisperse aggregates; b: small monodisperse aggregates; c: polydisperse aggregates (t_0: stop of agitation or starting time of settling)

Figure 5a: Aggregation of 0.5 μm silica in water followed by settling (pH = 3, λ = 550 nm) (1: 800 rpm; 2: 600 rpm; 3: 400 rpm; 4: 200 rpm)

Figure 5b: Aggregation of 1.5 μm silica in water followed by settling (pH = 3, λ = 550 nm)

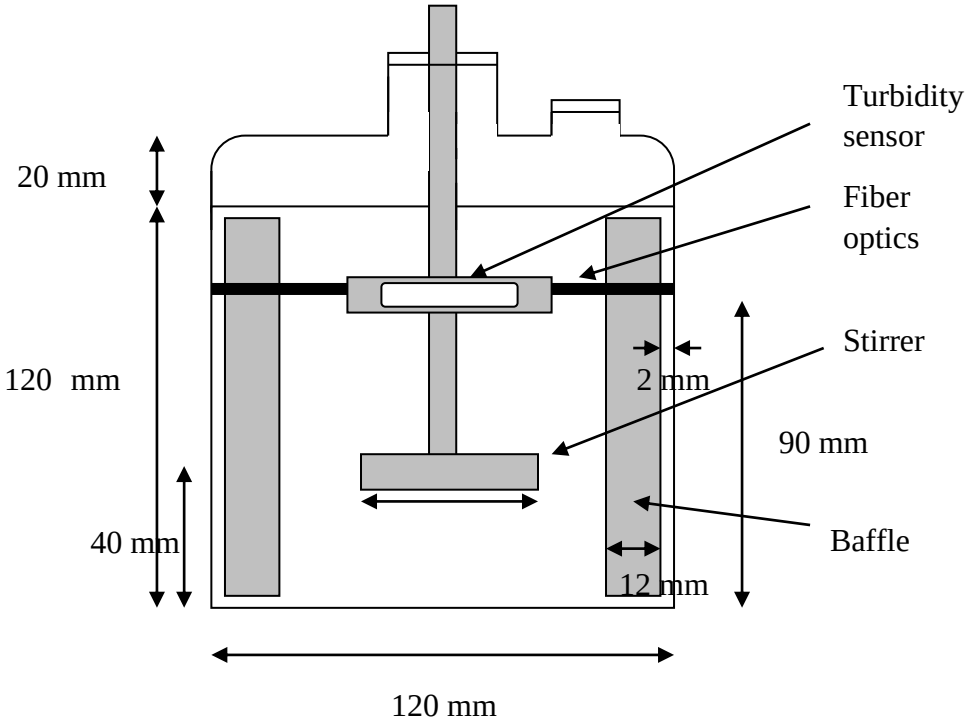

Figure 1: Schematic representation of the aggregation reactor

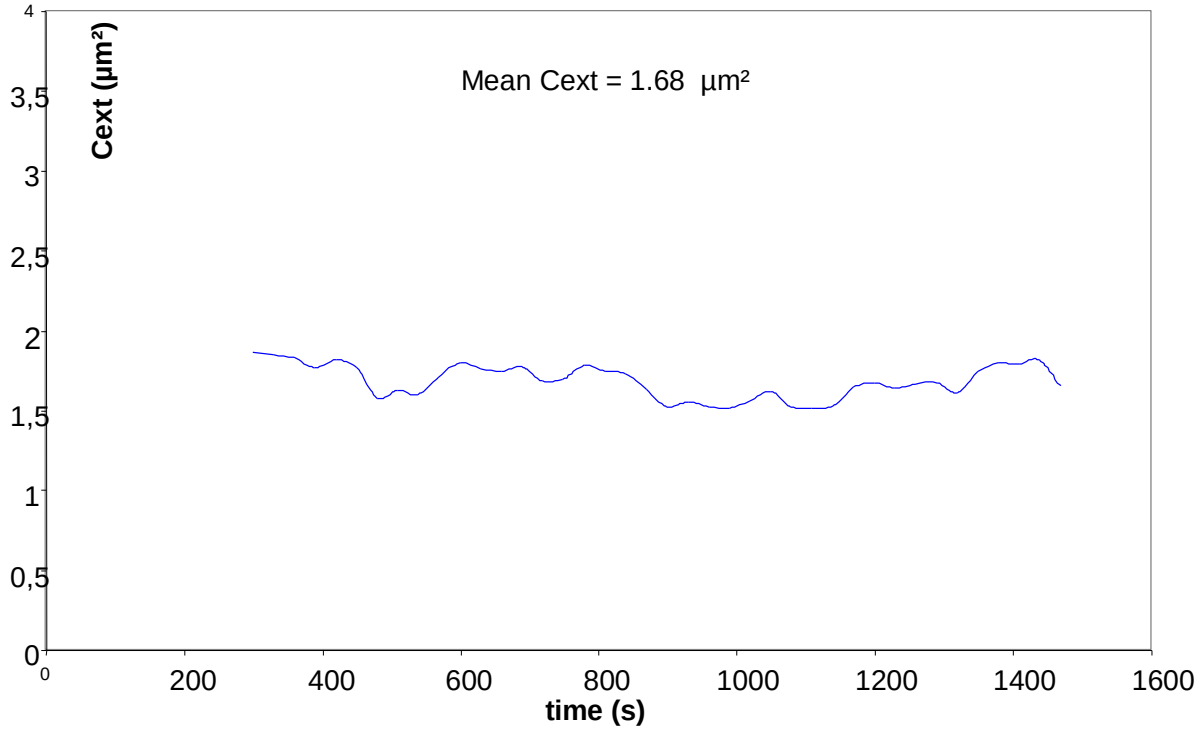

Figure 2: Extinction cross section versus time obtained by turbidity fluctuations analysis for 1.5 µm silica particles (pH = 8)

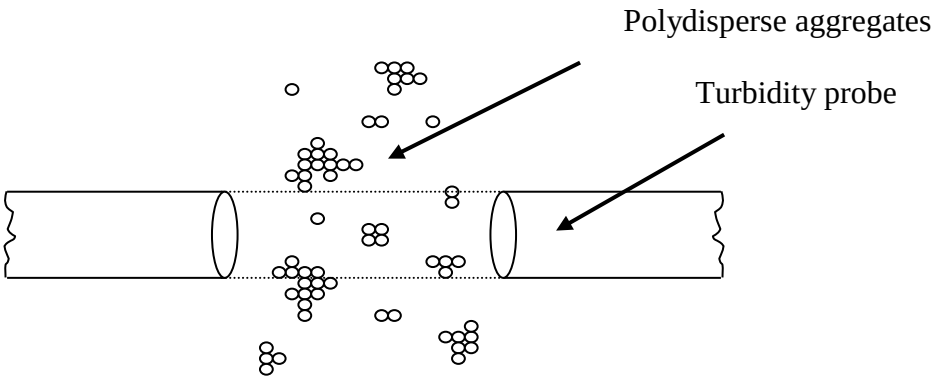

Figure 3: Aggregate settling as detected by the turbidity sensor

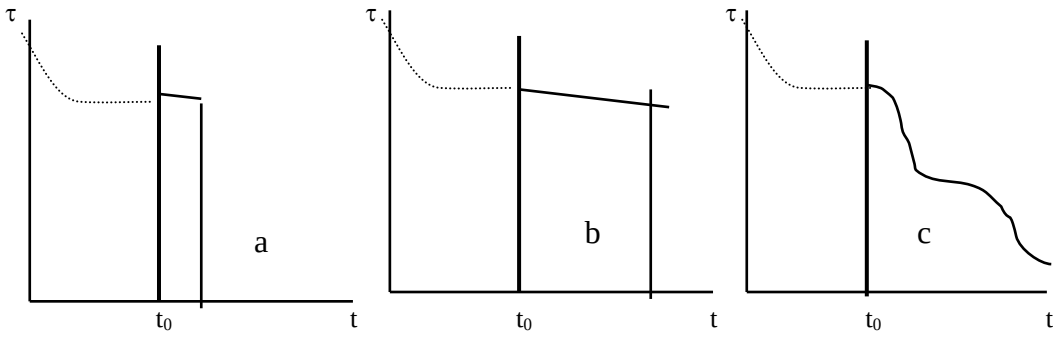

Figure 4: Turbidity variation during aggregate sedimentation; a: large monodisperse aggregates; b: small monodisperse aggregates; c: polydisperse aggregates. (t_0: stop of agitation or starting time of settling)

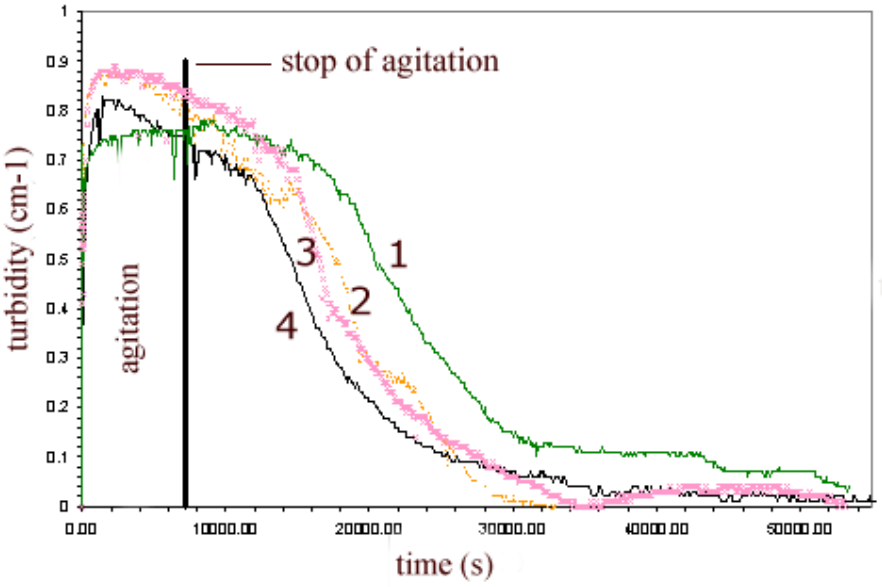

Figure 5a: Aggregation of 0.5 μm silica in water followed by settling (pH = 3, λ = 550 nm)

(1: 800 rpm; 2: 600 rpm; 3: 400 rpm; 4: 200 rpm)

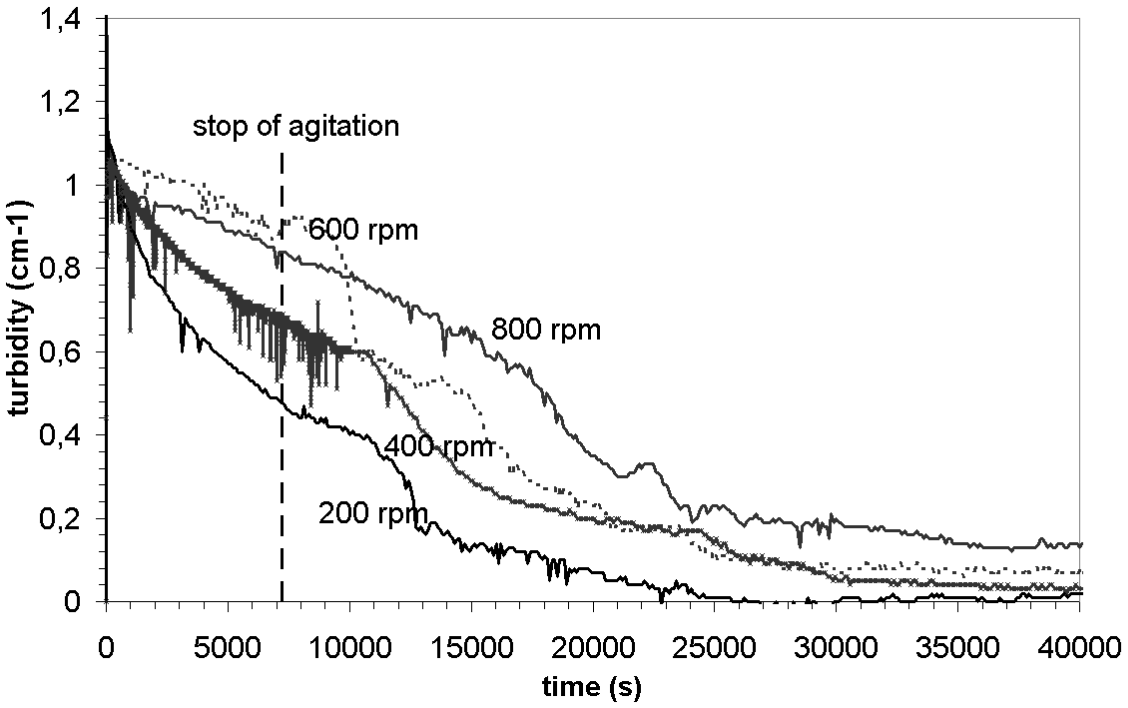

Figure 5b: Aggregation of 1.5 μm silica in water followed by settling (pH = 3, λ = 550 nm)

Table 1: Average experimental settling time, average primary particles number per aggregate, characteristic time for Brownian and settling aggregation

Silica	Settling time (s)	$\bar{i}_0$	T_{Ba} (s)	T_{sa} (s)
0.5μm	25000	50	$1.8\ 10^4$	389
1.5μm	10000	15	$1.15\ 10^5$	314

Table 2a: Normalized experimental settling velocity of silica aggregates formed at different stirring rates (silica 0.5μm)

Stirring rate (rpm)	Settling time(s)	v/v_1	$\bar{i}_0$
200	25900	10.0	61
400	26400	9.83	59
600	24300	10.7	68
800	24300	10.7	68

Table 2b: Normalized experimental settling velocity of silica aggregates formed at different stirring rates (silica 1.5μm)

Stirring rate (rpm)	Settling time(s)	v/v_1	$\bar{i}_0$
200	6000	5.8	24
400	8000	4.4	15
600	13000	2.7	6
800	15400	2.3	5

Table 3a: Estimation of the mean number of silica particles per aggregate (silica 0.5μm) by turbidity fluctuations analysis

Stirring rate (rpm)	200	400	600	800
C_{ext} (μm^2)	*6.7*	*4.7*	*2.7*	*2.7*
$C_{ext} \rightarrow L$	163	105	58	58
n	*785*	*1300*	*2430*	*2430*
n_0/n (= L)	162	98	52	52

Table 3b: Estimation of the mean number of silica particles per aggregate (silica 1.5μm) by turbidity fluctuations analysis

Stirring rate (rpm)	200	400	600	800
C_{ext} (μm^2)	*23*	*14*	*6*	*5*
$C_{ext} \rightarrow L$	24	13	4-5	3-4
n	*230*	*460*	*1050*	*1500*
n_0/n (= L)	26	13	5-6	4

Table 4a: Comparison of the mean number of silica particles per aggregate (silica 0.5μm) obtained by different methods

Stirring rate (rpm)	200	400	600	800
$C_{ext} \rightarrow L$	163	105	58	58
n_0/n (= L)	162	98	52	52
Particle number (from image analysis)	39	96	13	…
Particle number (from settling data)	61	59	68	68
Particle number (from aggregation modelling)	68	80	70	2

Table 4b: Comparison of the mean number of silica particles per aggregate(silica 1.5μm) obtained by different methods

Stirring rate (rpm)	200	400	600	800
$C_{ext} \rightarrow L$	24	13	4-5	3-4
n_0/n (= L)	26	13	5-6	4
Particle number (from image analysis)	46	…	25	20
Particle number (from settling data)	24	15	6	5
Particle number (from aggregation modelling)	17	5	2	4